RSC Advances

ROYAL SOCIETY OF CHEMISTRY

www.rsc.org/advances

A comparative study of CO oxidation reaction over pristine and C-doped boron nitride fullerene

Mehdi D. Esrafili*, Parisa Nematollahi, Roghaye Nurazar

Laboratory of Theoretical Chemistry, Department of Chemistry, University of Maragheh, Maragheh, Iran

E-mail: esrafili@maragheh.ac.ir (Mehdi D. Esrafili); *Corresponding author. **Tel. No:** (+98) 4212237955, **Fax:** (+98) 4212276060, **P.O. Box:** 5513864596.

Abstract

In this work, we employ density functional theory calculations to investigate the CO oxidation mechanisms over the $B_{12}N_{12}$ and $B_{11}N_{12}C$ nanocages. Two possible reaction pathways can be proposed for the oxidation of CO with O_2 molecule over these surfaces: $CO + O_2 \rightarrow OOCO \rightarrow CO_2 + O_{ads}$ and $CO + O_{ads} \rightarrow CO_2$. Both Eley–Rideal (ER) and Langmuir–Hinshelwood (LH) mechanisms are considered for these two reaction pathways. Our calculations indicate that the CO oxidation reaction over the $B_{11}N_{12}C$ nanocage proceeds via the ER mechanism followed by LH mechanism with an activation energy (E_{act}) of 0.58 eV. In the case of $B_{12}N_{12}$ nanocage, it can be estimated that the both reaction pathways go through the LH mechanism. The E_{act} of the first reaction step is about 2.5 eV, while it is negligible for the second route. Based on the present theoretical results, the catalytic activity of $B_{11}N_{12}C$ nanocage toward the CO oxidation reaction is more than that of $B_{12}N_{12}$ cluster. This can be related to the presence of C atom that plays a significant role in the activation of the whole cluster. Meanwhile, the performance of $B_{11}N_{12}C$ nanocage as a catalyst used for the oxidation of CO with O_2 molecule may be proceeded at near ambient temperatures. These results indicate that the $B_{11}N_{12}C$ nanocage can be utilized as a favorable low-cost catalyst for CO oxidation reaction.

Keywords: CO oxidation reaction, $B_{12}N_{12}$ nanocage, C-doping, DFT, $B_{11}N_{12}C$ nanocage, ER mechanism, LH mechanism

1. Introduction

The catalytic oxidation of carbon monoxide (CO) to carbon dioxide (CO_2) has long been a major reaction in heterogeneous catalysis. CO is a colourless and odourless but extremely toxic gas that is mainly produced by incomplete burning of fuels in automobiles and industrial processes.[1-3] When inhaled, it combines irreversibly with hemoglobin to produce carboxyhemoglobin, which its formation prevents the normal transfer of oxygen to body tissues. Thus, plentiful efforts have been done to oxidize the CO molecule by various noble metals such as Au,[4] Pd,[5,6] Pt [7] and Rh.[6] For instance, Alavi *et al.* [9] found that the CO oxidation over Pt (111) proceeds via an energy barrier of 1.00 eV, while it was reported by Stampfl and Scheffler to be about 1.02 eV over Ru(0001). [10] In another work, Haruta *et al.* [11] reported that Au catalysts supported on a metal oxide surface exhibit high catalytic activity for CO oxidation at low temperature. However, despite their high activity and selectivity toward the CO oxidation, these noble metal catalysts are rare and very expensive. Therefore, decreasing or substituting of these expensive noble metal-based materials with low-cost catalysts is one of the main important steps for the large-scale practical application of the catalytic CO oxidation process.[7]

Recently, scientists have found that different kinds of nanostructures such as single-walled or multi-walled carbon nanotubes (CNTs),[12,13] graphene[14] or boron-nitride nanotubes (BNNTs)[15] have a great tendency toward the adsorption of toxic gas pollutants. These nanostructures are also a promising candidates to support metal atoms or clusters to realize new catalysts due to their large surface-to-volume ratio[14], and outstanding electrical, mechanical and thermal properties.[16] Hence, many theoretical and experimental studies have been performed about the oxidation of CO on these nanostructures. For example, in one experimental study, Yoo *et al.* showed that the catalytic properties of graphene sheet enhances with the interaction of Pt nanoclusters.[17] In another comparative theoretical investigation, Tang *et al.* reported that the surface activity of the Pt-embedded graphene is increased significantly toward the oxidation of CO molecule.[18] Wang *et al.* found a strong chemical interaction between CO molecule and Si-doped BNNTs in comparison with pristine BNNTs.[19]

After the discovery of C_{60},[20] numerous studies have been focused on this outstanding carbon-based material due to its unique electronic properties with potential applications in building nanodevices.[21,22] C_{60} displays the promising ability for gas storage which makes it acts as a chemical sensor.[23] In recent years, many theoretical and experimental studies have focused

on the possible fullerene-like structures.[24,25] They found that III-V compounds, especially the group III nitrides can be desirable nanoscaled materials due to their direct band gap which affords optical and magnetic characteristics. So, the III-V fullerene-like cages have been theoretically estimated and experimentally synthesized.[26-28] On the other hand, different III-V nanostructures such as BNNTs,[29,30] BN nanosheets[31,32] and BN clusters,[33,34] with the unique polarity of B-N bonds, have more improved surface reactivity than carbon nanostructures. In particular, $(BN)_n$ (n=4-30) nanocages have been extensively investigated because of their high temperature stability, large thermal conductivity, oxidation resistance and low electric constant.[35,36] For example, Nigam *et al.* have shown that a chemically inert $(BN)_{36}$ cluster can be activated by incorporating magnetic nanoparticles inside it.[37] Therefore, the adsorption of O_2 molecule on these clusters results in an O–O bond elongation and then improves the CO oxidation reaction. Among these BN nanocages, the fullerene-like cage $B_{12}N_{12}$ as the smallest stable cage cluster is extensively investigated. Oku *et al.* experimentally synthesized the $B_{12}N_{12}$ nanocage by laser desorption time-of-flight mass spectrometry and reported that these clusters consists of 4- and 6-membered rings of BN with the band gap energy of about 5.1 eV.[38] On the other hand, there are several interesting investigations about the adsorption of chemical toxic gases on this favorable nanocage. For instance, in our previous work,[33] the adsorption and decomposition of methanol on $B_{12}N_{12}$ nanocage have studied in details. We found that the electrical conductivity of the $B_{12}N_{12}$ enhances upon the adsorption of CH_3OH and this nanocage could be used as an efficient metal-free catalyst for the dehydrogenation of the methanol molecule.

Today, chemical doping with foreign atoms is a favorable approach to modify the properties of host materials. In comparison with the undoped $B_{12}N_{12}$ cluster, C-doped BN fullerene ($B_{11}N_{12}C$) displays more reactivity than $B_{12}N_{12}$.[39-41] For example, Wu *et al.* showed that the hydrogenation reaction on $B_{11}N_{12}C$ cluster is both thermodynamically and kinetically favored under ambient conditions in which C atom acts as an activation center to dissociate H_2 molecule.[25] On the other hand, since the carbon atom has one less valence electron than nitrogen, the $B_{12}N_{11}C$ cluster exhibits the electron acceptor property around the carbon atom. Although this leads to an increase in the hydrogen chemisorption energy, but it makes a worse dehydrogenation property for the corresponding hydrogenated $B_{12}N_{11}C$ cage [40]. Furthermore, the adsorption and dehydrogenation of methanol on the $B_{11}N_{12}C$ surface was recently studied. [42] It is

found that the $B_{11}N_{12}C$ nanocage can effectively decompose the CH_3OH molecule with the carbon atom as an activation site. The results also indicated that in contrast to the $B_{12}N_{11}C$, more electrons can be transferred from the electron-rich $B_{11}N_{12}C$ to the CH_3OH molecule and thus lower activation energy can be achieved for the dehydrogenation reaction of the methanol on this cluster.

In this study, the oxidation of CO by O_2 molecule on the $B_{12}N_{12}$ and $B_{11}N_{12}C$ nanocages is investigated. Density functional theory (DFT) calculations are performed to show the strength and nature of the CO and O_2 interaction with the surface of these nanocages. The activation energies for the each reaction step on the $B_{12}N_{12}$ and $B_{11}N_{12}C$ cages are discussed and the corresponding mechanisms are compared. The results of this study could be useful for designing and developing metal-free catalysts based on BN nanostructures. To the best of our knowledge, the oxidation of CO molecule over $B_{12}N_{12}$ and $B_{12}N_{11}C$ nanocages is reported for the first time.

2. Computational details

All geometry optimizations and harmonic frequency calculations were performed at the M06-2X/6-31+G(2df, p) level of theory using the Gaussian 09 suite of programs.[43] Previous studies revealed that the M06-2X density functional is a reliable method for calculating the interaction energy and stability of noncovalent interactions.[44] Intrinsic reaction coordinate (IRC) calculations were performed in the forward and reverse directions to determine minimum-energy pathways. The adsorption energies (E_{ads}) of all the O_2/CO adsorbed nanocages were calculated as the difference between the total energy of the complexes and the energies of the corresponding isolated monomers at the M06-2X/6-31+G(2df, p) level. Both triplet and singlet spin states of O_2 molecule were considered. In order to check the thermodynamic feasibility of the adsorption process, the change of enthalpy (ΔH) and free-energy (ΔG) were obtained at 298.14 K and 1 atmosphere from the frequency calculations according to the following equations:

$$\Delta H = \sum_{\text{products}} (\varepsilon_0 + H_{corr}) - \sum_{\text{reactants}} (\varepsilon_0 + H_{corr}) \quad (1)$$

$$\Delta G = \sum_{\text{products}} (\varepsilon_0 + G_{corr}) - \sum_{\text{reactants}} (\varepsilon_0 + G_{corr}) \quad (2)$$

where ε_0 is the total electronic energy, while H_{corr} and G_{corr} are thermal corrections which should be added to ε_0 to obtain the enthalpy and Gibbs free energy, respectively.

3. Results and discussions

3.1. Geometric structures of $B_{12}N_{12}$ and $B_{11}N_{12}C$ clusters

First of all, the probable structure of fullerene-like nanocages $B_{12}N_{12}$ and $B_{11}N_{12}C$ are analyzed. The optimized structure of pristine $B_{12}N_{12}$ cage and its corresponding geometric parameters are shown in Figure 1. The $B_{12}N_{12}$ cage is the smallest stable BN fullerene[37] with T_h symmetry. The structural view of this small BN fullerene shows that this cluster contains from six 4-membered rings (4-MR) and eight 6-membered ring (6-MR) in which two individual B–N bonds exist: one is occupied by two 6-MRs and another by a 4-MR and a 6-MR. These bond lengths are about 1.44 and 1.48 Å, respectively, which are in good agreement with other related studies.[34,45,46] Considering the Mulliken charge density analysis indicates that the B and N atoms in $B_{12}N_{12}$ are positively and negatively charged with the same value of about 0.34 e, respectively. Therefore, these electron-deficient (B) and electron-rich (N) sites can be regarded as a Lewis acid and bases, respectively. When one carbon atom is substituted with the B atom in the $B_{12}N_{12}$ cluster, the $B_{11}N_{12}C$ nanocage is formed which its relaxed structure is depicted in Figure 1. One can see that after C-doping, the total geometry of $B_{11}N_{12}C$ is not significantly changed. The C–N bond length between two 6MRs decreases to 1.42 Å while the other one remains unchanged (1.48 Å). Upon C-doping, the charges redistribute on the BN cage, and the electron density is mainly accumulated around the C atom, which leads to the reduction of nearest B–N bonds length. Also, the ionic character of B–N bonds refers to a considerable electron transferring from B atoms to their adjacent N atoms. A great net charge of 0.84 e is transferred from the nearest N atoms to the C atom. Moreover, spin density analysis indicates that the spin density is mainly localized over the C atom while the small pockets of opposite spin are placed on the nearest N atoms. This provides further supports for the activation of $B_{12}N_{12}$ cluster by C-doping.

3.2. Adsorption of O_2 and CO molecules on the $B_{12}N_{12}$ and $B_{11}N_{12}C$ clusters

Before exploring the oxidation of CO by O_2 molecule, it is necessary to consider the adsorption of O_2 and CO molecules over $B_{12}N_{12}$ and $B_{11}N_{12}C$ cages, separately. Figure S1 of the Supporting Information displays the geometric parameters of the most energetically favorable configurations of triplet (complex **A**) and singlet O_2 (complex **B**) adsorbed over the $B_{12}N_{12}$ nanocage. Besides, Table 1 lists the corresponding binding distances (R), adsorption energies (E_{ads}), net charge-transfer (q_{CT}), spin density, and thermodynamic parameters (ΔG_{298} and ΔH_{298}) of these complexes. According to Figure S1, a triplet ground state of O_2 molecule is adsorbed in a tilted position over the $B_{12}N_{12}$ surface and forms the complex **A**. This is a common pattern for the adsorption of O_2 over different surfaces like Cu-[47] or Fe-doped[48] graphene and Si-doped

BNNTs.[49] It is clear from the large distance of B–O bond (2.7 Å) that the O_2 molecule is physically adsorbed over the $B_{12}N_{12}$ surface with a small E_{ads} value of -0.09 eV. The adsorption process to form complex **A** is exothermic (ΔH_{298} = -0.04 eV), but it has a positive ΔG_{298} value of about 0.28 eV which confirms that this adsorption process is not favorable at ambient conditions (Table 1). It can be also found from analysis of the spin density distribution (reported in Table 1) that the spin density is chiefly localized over the O_2 molecule (1.98 au). Additionally, the electron density difference (EDD) map of this configuration is depicted in Figure S1, while the red and blue colors display the charge accumulation and depletion, respectively. The obtained EDD plot shows that the electrons are depleted around the B–O bond and are accumulated in one O atom with a small net charge of about 0.08 e transfer from the gas molecule to the surface. These findings confirm that the interaction of O_2 molecule with the $B_{12}N_{12}$ surface is too weak to prevent desorption at room temperature. Moreover, it can be suggested that the O_2 adsorption has less effect on the electronic structure properties of the $B_{12}N_{12}$ due to the small E_{ads} and negligible charge transfer values.

On the other hand, complex **B** is achieved when a singlet spin state of O_2 molecule is considered. It is important to note that despite the larger E_{ads} (-0.21 eV) value of this complex, its total energy is smaller (less negative) than that of complex **A**. In addition, like complex **A**, this adsorption configuration is formed via an exothermic reaction while it is not a favorable reaction from the thermodynamic point of view (Table 1). In contrast with complex **A**, the EDD isosurface shows that the much more pronounced electron density is accumulated between the O_2 molecule and $B_{12}N_{12}$ (Figure S1). Also, a net charge of about 0.30 e is transferred from the $B_{12}N_{12}$ surface to the O_2 molecule which shows a stronger interaction between the B and O atoms than that in complex **A**.

Furthermore, CO molecule is found to be weakly adsorbed over the $B_{12}N_{12}$ cluster while it is placed in a vertical (end-on) position right above the B atom of the surface with the small E_{ads} of -0.10 eV (complex **C**). The B–C bond length of this configuration is about 1.79 Å. Although the formation of this complex is almost exothermic (ΔH_{298} = -0.06 eV), this is not a thermodynamically favorable reaction at room temperature ($\Delta G_{298} > 0$). There is also a small net charge (0.17 e) transferred from the CO molecule to the $B_{12}N_{12}$ surface, indicated that the CO molecule can be easily desorbs from the nanocage. It is also clear from the EDD map that a small electron density exists between the B atom of the surface and C atom of the CO molecule which

is originated from the large binding distance of B–C bond (Figure S1). Thus, it is predicted that the CO and triplet O_2 molecules can be simultaneously adsorbed over the $B_{12}N_{12}$ surface due to their similar adsorption energies.

The adsorption of individual O_2/CO molecules over the $B_{11}N_{12}C$ cage is also studied in detail. It should be mentioned that both triplet and singlet spin states of O_2 molecule are considered for the O_2 adsorption configuration. However, in both cases a doublet spin state is achieved. Figure S2 shows the most stable adsorption configuration of O_2 (configuration **D**) on the $B_{11}N_{12}C$ surface in which the O–O molecule is in parallel position to the surface right above the C atom and chemisorbs with the E_{ads} of -1.78 eV (Table S1). It is clear from the small C–O bond length (1.44 Å) and the large E_{ads} that there is a significant interaction between the O_2 molecule and the $B_{11}N_{12}C$ surface. In contrast to the nearly unchanged O–O bond length after adsorption of triplet and singlet O_2 over $B_{12}N_{12}$ cluster (complexes **A** and **B**), here, the O–O bond length of the adsorbed O_2 molecule is elongated to 1.30 Å which is due to the net charge of 0.19 e is transferred from the $B_{11}N_{12}C$ to the $2\pi^*$ orbitals of the O_2 molecule. It is clearly demonstrated in the EDD map in Figure S2 that a large electron density is accumulated around the C–O bond which confirms that there is a significant chemical interaction between the gas molecule and the C atom of the $B_{11}N_{12}C$ surface. These results indicate that the transferred electrons move from the C dopant to the adsorbed O_2 molecule. It should be noted that the adsorption of O_2 molecule on $B_{11}N_{12}C$ cluster is exothermic (ΔH_{298} = -1.71 eV). Also, it is a feasible reaction that can take place at room temperature (ΔG_{298} = -1.20 eV). Besides, the spin density distribution analysis shows that a large spin density is accumulated over the O2 molecule (0.98 au) rather than C atom (0.01 au) which provides an additional support for the activation of O_2 molecule over the $B_{11}N_{12}C$ cluster.

In the next step, the adsorption of a single CO molecule on the $B_{11}N_{12}C$ cluster is investigated. Complex **E** in Figure S2 shows that this molecule is adsorbed in the same geometric configuration with complex **C**, right above the B atom of the cluster with almost the same E_{ads} and B–O bond length values (Table 1). Like complex **C**, the formation of configuration **E** is exothermic while it is thermodynamically impossible at room temperature (Table S1). A net charge of about 0.01 e is transferred from the CO molecule to the $B_{11}N_{12}C$ cage. The EDD isosurface presented in Figure S2 indicates that the electron density is depleted around the B–C bond which is caused from the weak interaction between the CO molecule and

the $B_{11}N_{12}C$ surface.

In summary, comparing the E_{ads} values of the adsorbed O_2 molecule over the $B_{12}N_{12}$ and $B_{11}N_{12}C$ clusters clearly shows that the O_2 molecule is adsorbed more effectively over the $B_{12}N_{12}C$ cluster and has a larger effect on it. Also, the CO molecule is considered to be adsorbed on the $B_{11}N_{12}C$ surface later than the O_2 molecule due to its smaller (less negative) E_{ads} value. Therefore, in a mixture of O_2/CO molecules as the reaction gas, the $B_{11}N_{12}C$ surface will be chiefly covered by adsorbed O_2 molecules. So, the configuration **D** can be used as an initial state for the CO oxidation reaction.

3.3. The CO oxidation mechanisms over the $B_{12}N_{12}$ cluster

There are two well-established mechanisms for CO oxidation with O_2, namely, the Langmuir–Hinshelwood (LH) mechanism and the Eley–Rideal (ER) mechanism.[50,51] In the LH mechanism, the reaction occurs between the co-adsorbed O_2 and CO species, while in the ER mechanism, the CO molecule reacts directly with the activated O_2. To investigate the reaction of CO with O_2 over the $B_{12}N_{12}$ cluster, the geometry optimizations are carried out considering both LH and ER mechanisms. In order to study the CO oxidation mechanism over the $B_{12}N_{12}$ surface, the co-adsorbed CO and triplet spin state of O_2 molecules is chosen as an initial state because of their similar adsorption energies. Previous studies demonstrated that the type of catalyst determines the exact reaction pathway. For instance, Li *et al.* have found that the CO oxidation proceeds via the favorable ER mechanism with a two-step route, while the LH mechanism is not kinetically favorable.[51] Figure S3 demonstrates the minimum energy pathway of the CO oxidation reactions over the $B_{12}N_{12}$ cluster in which the following reactions are occurred:

$$O_2 + CO \rightarrow O_{ads} + CO_2 \quad (3)$$

$$O_{ads} + CO \rightarrow CO_2 \quad (4)$$

The corresponding activation energies (E_{act}) and reaction energies are also reported in Table 2. The local configurations of the gas molecules over the $B_{12}N_{12}$ cluster and their initial state (IS), transition state (TS) and final state (P) are depicted in Figure S4. The co-adsorbed O_2/CO molecules over the $B_{12}N_{12}$ surface forms the IS-1 in which both O_2 and CO molecules are adsorbed over the surface with corresponding B–O1 and B–C bond lengths of 2.85 and 1.78 Å, respectively (Figure S4). It is important to note that the estimated E_{ads} value for CO and O_2 co-adsorption on $B_{12}N_{12}$ (-0.20 eV) is slightly more negative than that the sum of individual adsorption energies of these species (-0.19 eV). In addition, the relatively small difference

between the adsorption energies of individual O_2 and CO molecules indicates that there is a certain probability of having O_2 and CO co-adsorbed on the $B_{12}N_{12}$. Then, the C atom of the CO molecule approaches to the O_2 atom and a peroxo-type structure O1–O2–C–O is produced (TS-1) over the $B_{12}N_{12}$ surface with the bond lengths of 1.34, 1.42 and 1.17 Å for O1–O2, O2–C and C–O, respectively (Figure S4). The activation energy (E_{act}) along the reaction pathway IS-1 → P-1 is 2.47 eV which is too high to proceeds rapidly at room temperature. Passing over the transition state TS-1, the formed CO_2 molecule with the E_{ads} value of -0.18 eV, desorbs easily from the surface, leaving an atomic oxygen (O_{ads}) adsorbed over the B atom of the $B_{12}N_{12}$ surface with the B–O_{ads} bond length and adsorption energy of 1.43 Å and -5.3 eV, respectively (Figure S4).

Considering the high energy barrier of the CO_2 formation via the LH mechanism (Figure S3), the question arises whether this pathway (IS-1→P-1) can be carried on via the ER mechanism. It is noteworthy that the E_{ads} of co-adsorbed O_2/CO molecules when they are proceeded via the ER mechanism in the triplet state of the O_2 molecule is about +1.26 eV which is not actually possible. Therefore, because of this positive E_{ads} value, the ER mechanism can't be considered for the first step.

In the following step, we check the activity of the atomic O_{ads} (O1) for CO oxidation via the LH mechanism. According to Figure S4, the configuration in which the C atom of the CO molecule is about 3.06 Å far away from the atomic O_{ads} is chosen as an IS-2. It is interesting to note that the P-2 is obtained via a barrier-less process. In TS-2, the O1–C–O complex is formed in a vertical position to the surface to facilitate the formation of CO_2 molecule (O1-C = 1.32 Å). Finally, in P-2, the second CO_2 molecule is formed which weakly interacted with the $B_{12}N_{12}$ (B–C = 2.99 Å) and hence can be easily released from the surface (E_{ads} = 0.21 eV). Generally, according to Table 2 and Figure S3, the reaction energy of these reaction steps (IS-1 → P-1 and IS-2 → P-2) are about -1.06 and -1.40 eV, respectively. It should be noted that since the second pathway with the LH mechanism proceeds via a barrier-less reaction, the ER mechanism does not consider for this reaction route.

Furthermore, the oxidation of CO molecule over the $B_{12}N_{12}$ surface is studied when the singlet O_2 is considered. The energy profile for the IS-3 → P-3 and IS-4 → P-4 reactions in which both LH and ER mechanisms are carefully studied is shown in Figure S5. Also, their local configurations along with some geometric values of the IS, TS and P are demonstrated in Figure

S6 and their corresponding thermodynamic values are listed in Table S1. The stable configuration for IS-3 is achieved in which the CO and O_2 molecules are adsorbed over the surface via the ER mechanism. In this configuration, a five-member ring is formed and the carbon atom of the CO molecule approaches to the O2 atom with the O2–C bond length of 1.35 Å. It should be noted that the E_{ads} of CO +O_2 in this complex (-4.12 eV) is more negative than that in complex **A** due to the formation of the stable five-member ring. So, this can be used as a favorable configuration in CO oxidation reaction. Because of the great stability of this complex, the TS-3 with the O2–C bond length of 2.03 Å is difficultly formed via the high E_{act} of about 3.35 eV which cannot be overcome at room temperature (Figure S5, Table S1). Passing from TS-3, the P-3 is obtained with the reaction energy of 2.41 eV. In this state, the atomic O_{ads} (O1) remains in the surface with the B–O1 bond length of 1.38 Å while the first CO_2 molecule is weakly interacted to the surface (N–C = 3.04 Å) that can be released easily at ambient conditions. In the next pathway, another CO molecule is adsorbed over the $B_{12}N_{12}$ surface via the LH mechanism and forms the IS-4. Herein, the B–C bond length is about 1.76 Å and the carbon atom is about 2.83 Å far from the atomic O1. The CO_2 molecule is obtained passing from TS-4 with the small E_{act} of about 0.06 eV. It is clear from the P-4 configuration that the second CO_2 molecule can be easily desorbed from the $B_{12}N_{12}$ surface (Figure S6).

3.4. The CO oxidation mechanisms over the $B_{11}N_{12}C$ cluster

Continually, the CO oxidation reaction is carefully investigated over the $B_{11}N_{12}C$ surface with both LH and ER mechanisms. First, the ER mechanism is considered. The related energy profile for the CO oxidation reaction pathways IS-5 → P-5 and IS-6 → P-6 over the $B_{11}N_{12}C$ nanocage are shown in Figure S7. The atomic configurations at various states along the reaction pathways are demonstrated at Figure S8. Beside, the corresponding E_{act} and reaction energy of these reaction pathways are summarized in Table 2. In the case of ER pathway, the gas-phase CO molecule is directly interacted with the adsorbed O_2 molecule. As it is clear from Figure S8, in the IS-5, CO molecule is physically adsorbed a little far away from the pre-adsorbed O_2 molecule with the O2–C bond length of 1.35 Å. Subsequently, the CO molecule approaches to the activated O_2 molecule in order to form TS-5 with the O2–C distance of 1.77 Å. Finally, a physisorbed CO_2 molecule is generated, with the E_{ads} value of -0.2 eV, which can be easily released from the cluster surface. Also, the O_{ads} (O1) is remained above the C atom of the $B_{11}N_{12}C$ surface while its adsorption energy is about 2 eV more negative than that between the O

and B atom of $B_{12}N_{12}$ cluster. This process is very close to the proposed ER pathway on the Si-doped BNNTs [52] or N- [53] and Sn-doped graphene [54]. Although the reaction energy of this step is about -3.10 eV, but it is not a barrier-less pathway (E_{act}=0.58 eV). Comparing with the moderate barrier of IS-7 → P-7 pathway (1.48 eV) followed by the LH mechanism (Figure S9 and Table S1), the ER mechanism is the favorable pathway for the CO oxidation over the $B_{11}N_{12}C$ nanocage which is likely to take place at low temperature.

In the following, the reaction between the CO and the atomic oxygen is carefully studied based on the LH mechanism via the IS-6 → P-6 pathway (Figures S7 and S8). Once the first formed CO_2 molecule leaves from the surface of nanocage, the second CO is supposed to be co-adsorbed with the O1 at the reaction site. In the IS-6, the C–O1 bond is about 1.37 Å while the CO molecule is physically adsorbed over the B atom of the $B_{11}N_{12}C$ cluster (B–C = 1.81 Å) while it is about 3.24 Å far away from the atomic O1. Attacking of O1 to the carbon atom of CO molecule generates TS-6 with the O1–C distance of 1.97 Å. The energy barrier equal to 0.09 eV is needed for the IS-6 → TS-6 reaction (Table 2). Like before, the CO_2 molecule is weakly interacted with the surface (E_{ads} = 0.1 eV and C–C = 3.04 Å), so, the CO_2 molecule can effectively desorbs from the $B_{11}N_{12}C$ surface and the $B_{11}N_{12}C$ catalyst can thus be recovered for a new round of CO oxidation.

For the ER mechanism, the process IS-6 → P-6 is completely different. As shown in Figures S9 and S10, the CO molecule is weakly adsorbed over the $B_{11}N_{12}C$ surface (O1-C = 2.73 Å) and considered as the IS-8. In this state, the C atom of the CO molecule attacks the O1 to generate TS-8 while the distance between the atomic O1 and C atom of the CO molecule is decreased from 2.73 to 1.97 Å. The E_{act} of this reaction is calculated about 0.21 eV which is significantly larger than that in LH mechanism (0.09 eV). At the end, the final product CO_2 is formed over the $B_{11}N_{12}C$ cluster and released from the surface at room temperature. Interestingly, it can be suggested that the oxidation of CO molecule over the $B_{11}N_{12}C$ is preferred to proceed via the ER mechanism followed by LH mechanism.

Based on the present theoretical results, the catalytic activity of $B_{11}N_{12}C$ nanocage toward the oxidation of CO molecule is more than that in $B_{12}N_{12}$ cluster due to the existence of C atom as an activation site. Moreover, the corresponding activation energy barriers of these mechanisms are significantly lowered compared with the undoped $B_{12}N_{12}$ case. Meanwhile, the performance of $B_{11}N_{12}C$ nanocage as a catalyst used for the oxidation of CO with O_2 molecule

may be proceed at near ambient temperatures.

4. Conclusion

In summary, the catalytic properties of pristine and C-doped $B_{12}N_{12}$ fullerene-like nanocages for the CO oxidation reaction were studied by means of DFT calculations. The equilibrium geometries and adsorption behavior of O_2 and CO molecules adsorbed on these nanocages were also identified. Both triplet and singlet spin states of the O_2 molecule were considered. Moreover, the CO oxidation reaction over these two different nanocages was studied via the ER and LH mechanisms, separately. Comparing the O_2/CO adsorption configurations over the $B_{11}N_{12}C$ cluster revealed, the adsorption of O_2 molecule is more favorable than the CO molecule. It should be noted that in contrast to $B_{12}N_{12}$, the O_2 adsorption over the $B_{11}N_{12}C$ cluster has a larger effect on electronic structure properties of the nanocage due to its larger E_{ads} and charge-transfer. In addition, a chemisorbed triplet O_2 molecule is more stable than the singlet one. Therefore, the triplet ground state of O_2 molecule was considered for the investigation of the CO oxidation reaction. Furthermore, it is found that the CO oxidation reaction over the $B_{11}N_{12}C$ nanocage is favorably proceeded via the ER mechanism followed by LH mechanism with the E_{act} of about 0.58 eV, while it proceeds through the LH mechanism in both pathways over the $B_{12}N_{12}$ cage (E_{act} = 2.47 eV). According to obtained results, it can be concluded that the $B_{11}N_{12}C$ cluster may be utilized as a favorable low-cost catalyst for CO oxidation reaction.

Reference

1. E. J. Peterson, A. T. De La Riva, S. Lin, R. S. Johnson, H. Guo, J. T. Miller, J. H. Kwak, C. H. F. Peden, B. Kiefer, L. F. Allard, F. H. Ribeiro and A. K. Datye, *Nat. Commun*., 2014, **5**, 1-11.

2. S. Royer and D. Duprez, *ChemCatChem,* 2011, **3**, 24–65.

3. H. J. Freund, G. Meijer, M. Scheffler, R. Schlögl and M. Wolf, *Angew. Chem. Int. Ed.,* 2011, **50**, 10064–10094.

4. N. Lopez, T. V. W. Janssens, B. S. Clausen, Y. Xu, M. Mavrikakis, T. Bligaard and J. K. Nørskov, *J. Catal*., 2004, **223**, 232–235.

5. X. Q. Gong, Z. P. Liu, R. Raval and P. Hu, *J. Am. Chem. Soc.*, 2004, **126**, 8–9.

6. I. Nakai, H. Kondoh, T. Shimada, A. Resta, J. N. Andersen and T. Ohta, *J. Chem. Phys*., 2006, **124**, 224712.

7. K. Bleakley and P. Hu, *J. Am. Chem. Soc.*, 1999, **121**, 7644–7652.

8. M. S. Chen, Y. Cai, Z. Yan, K. K. Gath, S. Axnanda and D. W. Goodman, *Surf. Sci*., 2007, **601**, 5326–5331.

9. A. Alavi, P. Hu, T. Deutsch, P. L. Silvestrelli and J. Hutter, *Phys. Rev. Lett*., 1998, **80**, 3650–3653.

10. C. Stampfl and M. Scheffler, *Phys. Rev. Lett*., 1997, **78**, 1500–1503.

11. M. Haruta, T. Kobayashi, H. Sano and N. Yamada, *Chem. Lett*., 1987, **2**, 405–408.

12. S. Furmaniak, A. P. Terzyk, P. A. Gauden, R. P. Wesołowski and P. Kowalczyk, *Phys. Chem. Chem. Phys.,* 2009, **11**, 4982-4995.

13. J. Gao and Y. L. Loo, *Phys. Chem. Chem. Phys., 2014,* **16**, 10861-10865.

14. K.S. Novoselov, A. K. Geim, S. V. Morozov, D. Jiang, Y. Zhang, S. V. Dubonos, I. V. Grigorieva and A. A. Firsov, *Science,* 2004, **306**, 666-669.

15. S. Lin, X. Ye and J. Huang, *Phys. Chem. Chem. Phys*., 2015, **17**, 888-895.

16. M. Cinke, J. Li, C. W. Bauschlicher, A. Ricca and M. Meyyappan, *Chem. Phys. Lett.,* 2003, **376**, 761-766.

17. E. Yoo, T. Okata, T. Akita, M. Kohyama, J. Nakamura and I. Honma, *Nano Lett.,* 2009, **9**, 2255-2259.

18. Y. Tang, Z. Yang and X. Dai, *Phys. Chem. Chem. Phys*., 2012, **14**, 16566–16572.

19. R. Wang and D. Zhang, *Aust. J. Chem.,* 2009, **61**, 941-945.

20. H. W. Kroto, J. R. Heath, S. C. O'Brien, R. F. Curl and R. E. Smalley, *Nature,* 1985, **318**, 162-163.

21. R. Czochara, P. Ziaja, P. Piotrowski, R. Pokrop and G. Litwinienko, *Carbon,* 2012, **50**, 3943-3946.

22. É. Tóth, R. D. Bolskar, A. Borel, G. González, L. Helm, A. E. Merbach and L. J. Wilson, *J. Am. Chem. Soc.,* 2005, **127**, 799-805.

23. M. K. Shukla, M. Dubey, E. Zakar, R. Namburu and J. Leszczynski, *Chem. Phys. Lett*., 2010, **493**, 130-134.

24. Q. Sun, Q. Wang and P. Jena, *Nano Lett.,* 2005, **5**, 1273-1277.

25. H. Wu, X. Fan and J. Kuo, *Int. J. Hydrogen Energ.,* 2012, **37**, 14336-14342.

26. C. Balasubramanian, S. Bellucci, P. Castrucci, M. De Crescenzi and S. V. Bhoraskar, *Chem. Phys. Lett.,* 2004, **383**, 188-191.

27. H. S. Wu, F. Q. Zhang, X. H. Xu, C. J. Zhang and H. Jiao, *J. Phys. Chem. A.,* 2003, **107**, 204-209.

28. A. Soltani, S. G. Raz, M. R. Taghartapeh, A. V. Moradi and R. Z. Mehrabian, *Comput. Mater. Sci.,* 2013, **79**, 795-803.

29. H. Choi, Y. C. Park, Y. H. Kim and Y. S. Lee, *J. Am. Chem. Soc.,* 2011, **133**, 2084-2087.

30. M. D. Esrafili and R. Nurazar, *Appl. Surf. Sci*., 2014, **314**, 90–96.

31. E. C. Anota, A. R. Juárez, M. Castro and H. H. Cocoletzi, *J. Mol. Model.,* 2013, **19**, 321-328.

32. J. Beheshtian, H. Soleymanabadi, A. A. Peyghan and Z. Bagheri, *Appl. Surf. Sci*., 2013, **268**, 436-441.

33. M. D. Esrafili and R. Nurazar, *Superlattice Microstruct.,* 2014, **67**, 54-60.

34. M. D. Esrafili and R. Nurazar, *Surf. Sci.,* 2014, **626**, 44–48.

35. D. B. Zhang, E. Akatyeva and T. Dumitrică, *Phys. Rev. B.,* 2011, **84**, 115431.

36. D. L. Strout, *J. Phys. Chem. A*., 2001, **105**, 261-263.

37. S. Nigam and C. Majumder, *ACS Nano,* 2008, **2**, 1422-1428.

38. T. Oku, A. Nishiwaki and I. Narita, *Sci. Technol. Adv. Mater.,* 2004, **5**, 635-638.

39. A. W. van den Berg and C. O. Areán, *Chem. Commun.,* 2008, **6**, 668-681.

40. H. Y. Wu, X. F. Fan, J. L. Kuo and W. Q. Deng, *Chem. Commun.,* 2010, **46,** 883–885.

41. M. D. Esrafili and R. Nurazar, *J. Cluster Sci.,* 2015, ***26***, 595-608.

42. M. D. Esrafili and R. Nurazar, *Comput. Mater. Sci.,* 2014, **92**, 172-177.

43. M. J. Frisch, G. W. Trucks, H. B. Schlegel, G. E. Scuseria, M. A. Robb, J. R. Cheeseman, G. Scalmani, V. Barone, B. Mennucci, G. A. Petersson, H. Nakatsuji, M. Caricato, X. Li, H. P. Hratchian, A. F. Izmaylov, J. Bloino, G. Zheng, J. L. Sonnenberg, M. Hada, M. Ehara, K. Toyota, R. Fukuda, J. Hasegawa, M. Ishida, T. Nakajima, Y. Honda, O. Kitao, H. Nakai, T. Vreven, J. A. Montgomery, Jr, J. E. Peralta, F. Ogliaro, M. Bearpark, J. J. Heyd, E. Brothers, K. N. Kudin, V. N. Staroverov, R. Kobayashi, J. Normand, K. Raghavachari, A. Rendell, J. C. Burant, S. S. Iyengar, J. Tomasi, M. Cossi, N. Rega, J. M. Millam, M. Klene, J. E. Knox, J. B. Cross, V. Bakken, C. Adamo, J. Jaramillo, R. Gomperts, R. E. Stratmann, O. Yazyev, A. J. Austin, R. Cammi, C. Pomelli, J. W. Ochterski, R. L. Martin, K. Morokuma, V. G. Zakrzewski, G. A. Voth, P. Salvador, J. J. Dannenberg, S. Dapprich, A. D. Daniels, Ö. Farkas, J. B. Foresman, J. V. Ortiz, J. Cioslowski, and D. J. Fox, 2009, Gaussian, Inc, Wallingford CT.

44. Y. Zhao and D. G. Truhlar, *Theor. Chem. Acc.,* 2008, **120**, 215-241.

45. S. Yourdkhani, T. Korona and N. L. Hadipour, *J. Phys. Chem. A.,* 2015, **119**, 6446–6467.

46. F. Zhao, Y. Wang, M. Zhu and L. Kang, *RSC Adv.,* 2015, **5**, 56348-56355.

47. E. H. Song, Z. Wen and Q. Jiang, *J. Phys. Chem. C.,* 2011, **115**, 3678–3683.

48. Y. F. Li, Z. Zhou, G. T. Yu, W. Chen and Z. F. Chen, *J. Phys. Chem. C.,* 2010, **114**, 6250–6254.

49. M. D. Esrafili and N. Saeidi, *Struct. Chem.,* 2015, DOI: 10.1007/s11224-015-0590-z.

50. T. Engel and G. Ertl, *J. Chem. Phys.,* 1987, **69**, 1267-1281.

51. F. Li, J. Zhao and Z. Chen, *J. Phys. Chem. C.,* 2012, **116**, 2507-2514.

52. M. D. Esrafili, N. Saeidi and P. Nematollahi, *RSC Adv.* 2015, **5**, 100290.

53. M. D. Esrafili, R. Mohammad-Valipour, S.M. Mousavi-Khoshdel, P. Nematollahi, *ChemPhysChem* 2015, **16**, 3719–3727.

52. M. D. Esrafili and N. Saeidi, Physica E 2015, **74**, 382-387.

Figure 1. Optimized structures of pristine $B_{12}N_{12}$ and $B_{11}N_{12}C$ clusters. All bond distances are in Å. Color code for each optimized structure: blue ball: N; brown ball: B; gray ball: C.

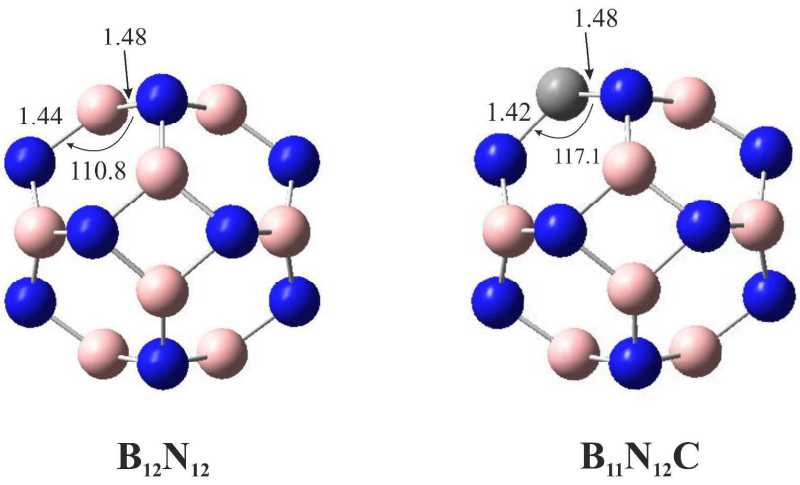

Table 1. Calculated binding distances (R), adsorption energy (E_{ads}), net charge-transfer (q_{CT}), spin density, change of Gibbs free energy (ΔG_{298}) and change of enthalpy (ΔH_{298}) of triplet O_2 (**A, D**), singlet O_2 (**B**) and CO (**C, E**) adsorption over $B_{12}N_{12}$ and $B_{11}N_{12}C$

surface	R (Å)	E_{ads} (eV)	q_{CT} (e)	spin density (au)	ΔG_{298} (eV)	ΔH_{298} (eV)
$B_{12}N_{12}$				-		
A	2.70	-0.09	0.08	1.98 [a]	0.28	-0.04
B	1.78	-0.21	0.30	-	0.24	-0.17
C	1.79	-0.10	0.17	-	0.37	-0.06
$B_{11}N_{12}C$				1.06 [b]		
D	1.44	-1.78	0.19	0.97 [a]	-1.20	-1.71
E	1.82	-0.07	0.01	-	0.39	-0.03

[a] The estimated spin density over O_2 molecule. [b] The estimated spin density over carbon atom of $B_{11}N_{12}C$.

Table 2. Calculated activation energy (E_{act}) and reaction energy (ΔE) for different pathways of CO oxidation by O_2 molecule over $B_{12}N_{12}$ and $B_{11}N_{12}C$ clusters

Reaction	E_{act} (eV)	ΔE (eV)
$B_{12}N_{12}$		
IS-1 → P-1	2.47	-1.06
IS-2 → P-2	-	-1.40
$B_{11}N_{12}C$		
IS-5 → P-5	0.58	-3.10
IS-6 → P-6	0.09	-1.51

Graphical abstract.